

This is a repository copy of Encapsulation of iodine-loaded adsorbents in blended Portland cement and geopolymer wasteforms.

White Rose Research Online URL for this paper: <a href="https://eprints.whiterose.ac.uk/id/eprint/232795/">https://eprints.whiterose.ac.uk/id/eprint/232795/</a>

Version: Published Version

# Article:

Simoni, M., Kearney, S.A., Robshaw, T.J. et al. (6 more authors) (2024) Encapsulation of iodine-loaded adsorbents in blended Portland cement and geopolymer wasteforms. Cement and Concrete Research, 179. 107480. ISSN: 0008-8846

https://doi.org/10.1016/j.cemconres.2024.107480

# Reuse

This article is distributed under the terms of the Creative Commons Attribution (CC BY) licence. This licence allows you to distribute, remix, tweak, and build upon the work, even commercially, as long as you credit the authors for the original work. More information and the full terms of the licence here: https://creativecommons.org/licenses/

# Takedown

If you consider content in White Rose Research Online to be in breach of UK law, please notify us by emailing eprints@whiterose.ac.uk including the URL of the record and the reason for the withdrawal request.



ELSEVIER

Contents lists available at ScienceDirect

# Cement and Concrete Research

journal homepage: www.elsevier.com/locate/cemconres





# Encapsulation of iodine-loaded adsorbents in blended Portland cement and geopolymer wasteforms

Marco Simoni <sup>a</sup>, Sarah A. Kearney <sup>a</sup>, Thomas J. Robshaw <sup>a,b</sup>, Joshua Turner <sup>c</sup>, Kyle O'Donoghue <sup>a</sup>, Daniel A. Geddes <sup>a</sup>, Clint A. Sharrad <sup>d</sup>, Mark D. Ogden <sup>a</sup>, Brant Walkley <sup>a,\*</sup>

- <sup>a</sup> Department of Chemical and Biological Engineering, The University of Sheffield, Mappin Street, Sheffield S1 3JD, UK
- <sup>b</sup> Faculty of Life Sciences, The University of Bradford, Bradford, West Yorkshire BD7 1DP, UK
- <sup>c</sup> National Nuclear Laboratory Ltd., Warrington Road, Birchwood Park, Warrington WA3 6AE, UK
- d Department of Chemical Engineering and Analytical Science, The University of Manchester, Oxford Road, Manchester, M13 9PL, UK

#### ARTICLE INFO

# Keywords: Radioiodine Radioactive waste immobilisation Portland cement Geopolymers Adsorption

#### ABSTRACT

Capture of radioiodine by solid adsorbents and subsequent cementation is a promising solution to achieve "Near Zero" emissions from nuclear fuel cycles. We investigate cementation of iodine-loaded silica adsorbents in blast furnace slag blended Portland cement (BFS:PC) and metakaolin-based geopolymers, and subsequent leaching in deionised water. Adsorbent encapsulation retarded BFS:PC hydration, but not geopolymer reaction. Phase assemblage was unaffected by adsorbent encapsulation for both BFS:PC and geopolymers, which comprised calcium aluminosilicate hydrate and potassium aluminosilicate hydrate gels, respectively. Adsorbents were encapsulated intact within BFS:PC, whereas adsorbents dissolved in the high pH of fresh geopolymers. BFS:PC exhibited low leaching stability and an alteration layer, however minimal iodine leaching occurred due to intact absorbents. Geopolymers showed high leaching stability, however adsorbent degradation resulted in significant iodine leaching. This evidences potential for cementation of radioiodine-loaded adsorbents under mild conditions, and highlights the importance of synergy when designing adsorbents and wasteforms for radioiodine abatement.

#### 1. Introduction

Despite the rapidly growing concern amidst readily observable effects of climate change, global energy demand is still primarily met by energy production based on burning fossil fuels, with 84 % of the global energy mix produced this way [1]. For the world to limit global warming to 2 °C by 2050 compared to pre-industrial levels a significant cut to the carbon emissions arising from the global energy sector is required [2]. The nuclear sector is expected to play a key role in achieving that ambition due to its high energy density, high capacity factor and low environmental impact [3]. Currently, the nuclear sector provides approximately 4 % of global energy demand [1], and this value is expected to increase before 2050 [4]. However, like many industrial processes, careful waste management is required to minimise the environmental impact and ensure its sustainability [5]. Consequently, in recent years, significant attention and resources have been focused on developing new options for the removal of hazardous elements, i.e. radioiodine, from the liquid streams arising of the reprocessing PUREX process (Fig. 1; the red arrows indicate the path of radioiodine).

There are two major radioiodine isotopes of concern. I-131 is a high energy beta- and gamma-emitter, but has a half-life of only ~8 days and therefore principal risks are confined to accidental mass environmental release. In contrast, I-129 is the focus of this work, as its half-life of 1.57  $\times$  10<sup>7</sup> years necessitates a clear strategy for long-term management. The majority (94-99 %) of the total radioiodine is volatilised upon dissolution of the SNF into nitric acid, and it may be found in the "dissolver offgas", while the remaining fraction of iodine is released through solvent extraction [6] and vitrification of the high-level waste (HLW) [7], within the central and waste off-gas, respectively. The capture of gaseous iodine (I2) can be achieved via wet scrubbing and solid adsorption [8], and extensive literature can be found for a wide range of relevant adsorbents, i.e. activated carbon [9], macroreticular resins [10], zeolites [11], and Ag-based materials [12]. Upon condensation of the volatile fraction, such liquid streams are discharged to the environment within strict regulatory limits, with the environmental impact of the contaminants released is accepted to be small in comparison with the cost of their

E-mail address: b.walkley@sheffield.ac.uk (B. Walkley).

<sup>\*</sup> Corresponding author.

removal. However, a "Near Zero" discharge policy within the future fuel cycle is strongly expected, and research is being carried out to develop technologies that can achieve this [13]. Efficient removal of iodine from the resulting solution might offer further alternatives, but the high pH and anionic competition limit the selectivity of the adsorbents for the targeted species. The use of commercially available ion-exchange materials appears promising given the enhanced selectivity achieved upon attachment of a hard Lewis acid, i.e. metal ions, through the so-called metalation step. Likely, events of in-situ salt precipitation and ligand-exchange are promoted given the enhanced affinity of the composite adsorbent for Lewis bases, i.e. iodine [14,15].

The disposal of the adsorbed radioiodine into geological repositories appears promising with respect to the current discharge policy; however, a suitable wasteform still needs development, and this depends on the properties of the materials to be immobilised. Due to the volatility of iodine, high-temperature processes such as vitrification may not be appropriate, whereas other techniques, such as low-temperature glass sintering [16] or Hot Isostatic Pressing [17] are expected to have greater applicability. However, technically complex processes and high costs require further investigation of alternatives, such as cementation which is characterised by mild operating conditions, simplicity of the process, ability to condition granular absorbent materials, and avoidance of volatilisation of radioiodine [18,19]. Traditionally, contaminated adsorbent materials have been encapsulated in Portland cement (PC) [20–22].

Geopolymers are a sub-group of alkali-activated materials (AAM), formed via reaction of an aluminosilicate precursor (e.g. calcined clays) with an alkaline source, resulting in polymerisation of aluminosilicate oligomers and formation of a solid binder (Fig. 2).

These materials exhibit certain characteristics, i.e. cation-binding sites, a tortuous pore network with low connectivity, chemical resistance to many radioactive waste streams, and compatibility with absorbent materials, may make them superior materials for the cementation of contaminated novel adsorbent materials. Geopolymers have already been investigated in these terms due to the pseudo-zeolitic nature of the N,K-A-S-H gel formed, leading to promising results such as the low-temperature formation of sodalite, which is an excellent candidate phase for long term chemical immobilisation of radioiodine [25], and is usually synthesised through energy-intensive or technically complex routes [26].

We previously assessed the capabilities of a number of organosilica adsorbents to capture iodine from aqueous conditions simulating industrially relevant waste streams, and concluded that mercapto and thiourea ligands, loaded with Ag and Cu, were the most promising absorbents [15,27]. Here, we encapsulate these iodine-loaded functionalised adsorbents in both BFS:PC and geopolymer cements, characterise their phase assemblage, micro and nanostructure, and assess their stability and iodine retention during prolonged leaching in deionised water. Using an array of advanced spectroscopic and microstructural characterisation approaches, this work reveals the encapsulation/incorporation mechanisms, mass transport processes, and iodine retention in these cement wasteforms. This information is essential to demonstrate that an iodine loaded capture material can be designed with a wasteform conversion step in mind to enable simplicity and synergy in the process. This may enable methods of iodine capture that further reduces iodine discharge and reduce secondary wastes, enabling future fuel recycling to achieve a potential "Near Zero" policy.

# 2. Materials and methods

#### 2.1. Materials

This study investigated development of cement wasteforms that can be used to encapsulate three different hybrid silica materials, chosen based on previously published work identifying optimum iodine uptake in the order of 100-150 mg per gram of adsorbent [15,27]. The candidates were: synthetized Mercaptsosilica (the synthesis method has been previously reported [15]), and commercially available MercaptoSil and TUPrSIL (PhosphonicS Ltd). The materials used in this work included reagent grade chemicals: Fluorochem KI (≥98.0 %), AgNO<sub>3</sub> (Sigma Aldrich, ≥99.0 %), CuCl<sub>2</sub>.2H<sub>2</sub>O (Sigma Aldrich, ≥99.9 %), Fisher Scientific KOH (99 %), and commercial grade potassium silicate solutions  $K_2SiO_3$  (PQ-KS, 51.6 mass%  $K_2SiO_3,$  with a  $SiO_2/$   $M_2O$  of 2.2). The wasteforms in this study were produced from Ketton coarse ground PC from Hanson Cement (UK), ground granulated blast furnace slag (BFS) from ECOCEM (France), and metakaolin (MetaMax, BASF and Lawrence Industries, UK), and we have previously published a preliminary investigation into the microstructural characteristics of similar cement wasteforms [28]. Chemical composition data for all solid raw materials were determined using X-ray fluorescence analysis, reported in Table 1; CaO, SiO<sub>2</sub> and Al<sub>2</sub>O<sub>3</sub> were the main oxides detected in all solid raw materials, with CaO/SiO2 dominant in PC and BFS, and SiO2/Al2O3 in MetaMax metakaolin.

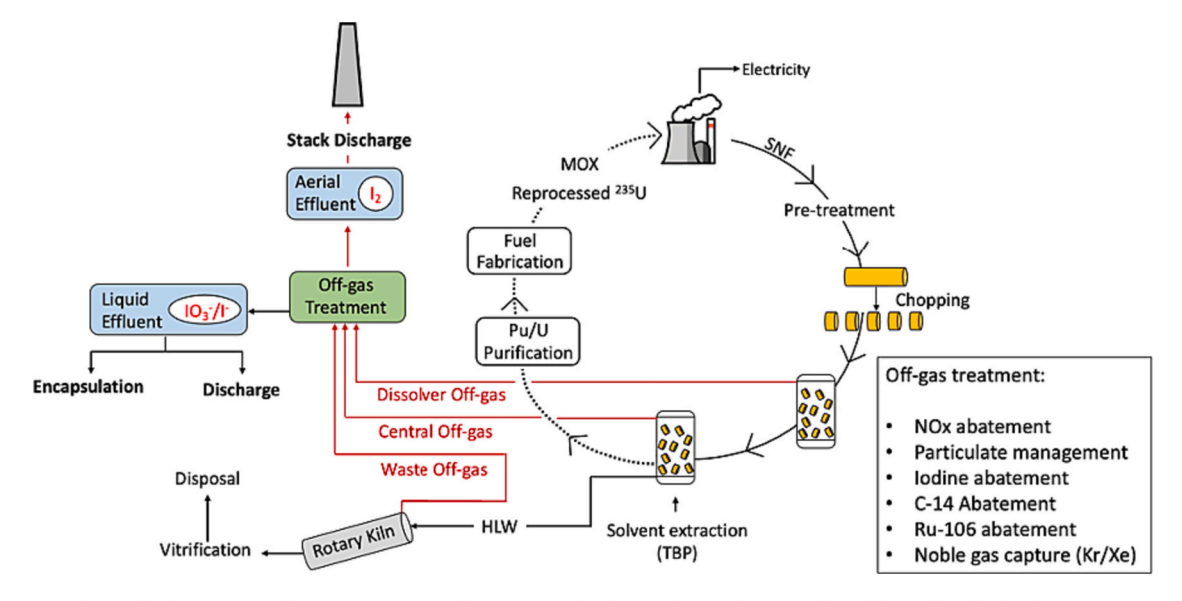


Fig. 1. Schematic and simplified overview of the PUREX process; the presence of iodine in the gas phase is reflected by red-highlighted arrows. (For interpretation of the references to colour in this figure legend, the reader is referred to the web version of this article.)

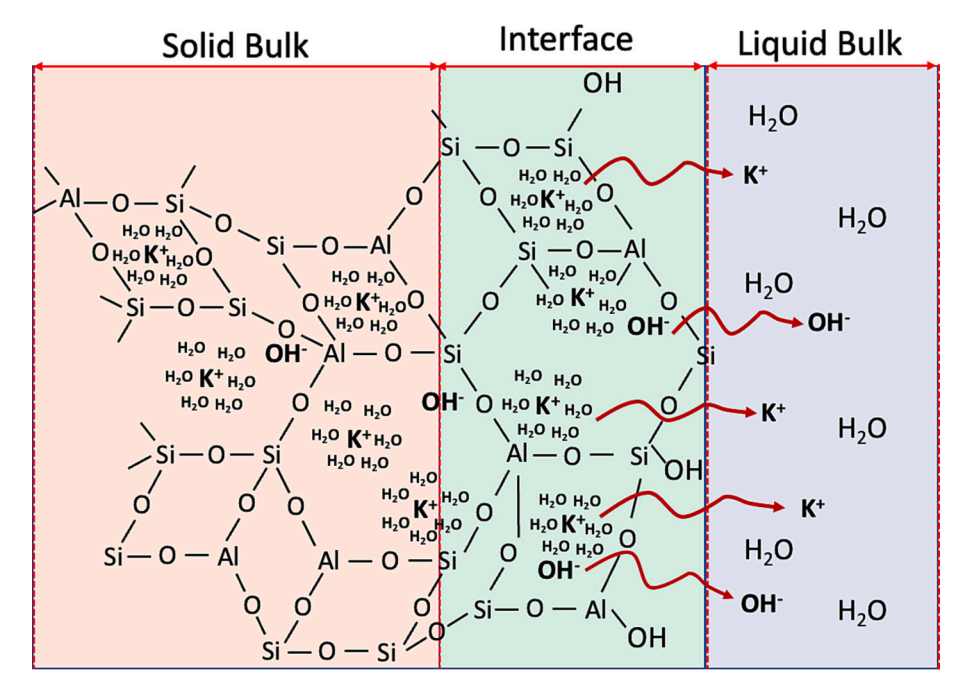


Fig. 2. Approximate structural arrangement of the geopolymer matrix produced upon reaction between the activating solution (K-based) and metakaolin (source of Al and Si).

Table 1
Oxide composition (mass %) determined by X-ray fluorescence for the materials used in this study. PC: Portland cement; BFS: blast furnace slag; Metamax metakaolin.

	PC (mass%)	BFS (mass%)	Metamax (mass%)
SiO <sub>2</sub>	21.6	36.0	52.5
$Al_2O_3$	5.1	11.3	44.5
$Fe_2O_3$	2.6	0.3	1.9
CaO	64.9	41.3	_
MgO	1.0	6.5	-
$TiO_2$	0.4	0.5	1.3
$SO_3$	2.6	0.7	-
Others <sup>a</sup>	1.6	0.7	0.4

<sup>&</sup>lt;sup>a</sup> Including K<sub>2</sub>O, Na<sub>2</sub>O, MnO, CI<sup>-</sup>.

# 2.2. Experimental procedure

#### 2.2.1. Adsorbent loading

Prior to metalation, all the adsorbents were conditioned in 1 M HNO<sub>3</sub> solutions for 24 h, following which they were rinsed and stored in deionised water until usage. The metalation was performed by dissolution of AgNO<sub>3</sub> or CuCl<sub>2</sub>.H<sub>2</sub>O into deionised water (0.1 M); 0.5 g of adsorbent was immersed into 50 mL of the solution containing the targeted metal ions. To achieve equilibrium, the systems were sealed and placed on an orbital shaker for 48 h; subsequently, the metalated adsorbents were rinsed and stored in deionised water. Considering a 2 mass % iodine uptake on the adsorbents, KI was dissolved into deionised water to have an iodine concentration of 1 g·L<sup>-1</sup>; 0.1 g of adsorbent was treated with 25 mL of solution on an orbital shaker for 48 h. Prior to the experiments, the adsorbents were washed with deionised water to remove any residual iodine from the solids. Aliquots of the solutions were sampled to assess the iodine loading performed through ion-selective electrode. For clarity, an overview is provided in Table 2 below.

The iodine uptake was calculated by considering the mass balance of the KI solutions used prior and upon treatment of the adsorbents, as reported in Eq. 1.

Table 2
Details of the adsorbents selected including iodine loading on the adsorbent, expressed in mg<sub>lodine</sub>/g<sub>Solids</sub>.

Adsorbent ID	Adsorbent name	lodine (mg/g)
M1 Ag	Mercaptosilica <sup>a</sup> + Ag	$58.4 \pm 2$
M2 <sup>-</sup> Ag	MercaptoSil + Ag	$72.9 \pm 5$
M2 <sup>·</sup> Cu	MercaptoSil + Cu	$32.8 \pm 5$
T <sup>-</sup> Ag	TUPrSIL+ Ag	$119.5\pm 5$
T'Cu	TUPrSIL+ Cu	$61.1 \pm 5$

<sup>&</sup>lt;sup>a</sup> Synthetised. All other hybrid silica materials purchased.

$$q_{e} = \left(C_{0} - C_{f}\right) \bullet V_{0} / m_{Adsorbent} \tag{1}$$

In Eq. 1,  $q_e$ ,  $C_0$ ,  $C_f$ ,  $V_0$ , and  $m_{Adsorbent}$  are defined as the amount of iodine adsorbed ( $mg/g_{Adsorbent}$ ), the concentration of iodine prior treatment with adsorbents, upon treatment with adsorbents, the initial volume of the KI used, and the mass (g) of the adsorbent introduced, respectively.

For the wasteforms based on PC blended with BFS, a 3 to 1 BFS:PC proportion was chosen to align with the formulation used in a Waste Encapsulation Plant (WEP) at the Sellafield nuclear site for treatment of barium carbonate wastes, including Co-Treat [29], and to also align with the formulation envelope for UK intermediate level waste (ILW) grouts. The Hanson PC used conformed to specifications set by Sellafield Ltd. (SL) [29]. Hydration was performed using a w/b ratio of 0.4, ensuring high compressive strength [30] while keeping the water content low to hinder the mobility of iodine. Firstly, the adsorbent was added to the deionised water for the reaction, and the PC and BFS powders were subsequently added. Addition of each component was controlled by mass. Manual mixing was initially used to ensure homogenisation, and the resulting paste was then mixed with a shear Heidolph overhead stirrer for 10 min at 400 rpm, with the mixing speed chosen to avoid the disintegration of the adsorbent. Finally, the paste was poured into 30 mL centrifuge plastic tubes, vibrated to remove entrapped air, and the sealed packages were cured at 20 °C for 28 days. For clarity, Table 3 below reports the samples produced starting from the BFS:PC formulation, also including a reference sample (BFS:PC\_Ctrl) prepared without

**Table 3**Overview of the BFS:PC samples prepared, highlighting the ID of the specimen, the adsorbent used, and the overall iodine uptake.

Sample ID	Adsorbent	lodine (mg/g)
BFS:PC'Ctrl	_	_
BFS:PC' M1'Ag	Mercaptosilica <sup>a</sup> + Ag	$1.1\pm2$
BFS:PC' M2'Ag	MercaptoSil + Ag	$1.4 \pm 5$
BFS:PC' M2'Cu	MercaptoSil + Cu	$0.6 \pm 5$
BFS:PC'T'Ag	TUPrSIL+ Ag	$\textbf{2.3} \pm \textbf{5}$
BFS:PC'T'Cu	TUPrSIL+ Cu	$1.2\pm 5$

a Synthetised.

#### adsorbent or iodine.

For the synthesis of the geopolymer wasteforms, samples were formulated as per previously published work [26]. The activator was prepared by mixing the potassium silicate activator with KOH solutions; the final stoichiometry of the solution was designed as follows: H<sub>2</sub>O/  $K_2O = 11$ ,  $SiO_2/K_2O = 1$ ,  $Al_2O_3/K_2O = 1$  and  $SiO_2/Al_2O_3 = 1$ . The MetaMax metakaolin was then added to the activating solution and initially hand-mixed to ensure homogenisation and to avoid agglomeration, and the resultant paste was subsequently mixed for 10 min with a shear Heidolph overhead stirrer at 400 rpm. As above, the mixing speed was chosen to avoid the disintegration of the adsorbents by mechanical friction. Overall, a water-to-binder (w/b) ratio of 0.5 was used, since these conditions have been identified to lead to high compressive strengths while retaining acceptable workability [31]. Table 4 below reports an overview of the geopolymer samples prepared, with GP\_Ctrl used as a reference and reflecting the geopolymer system without adsorbent or iodine.

# 2.2.2. Leaching tests

Cement samples were cured for 28 days at 20 °C, after which they were demoulded and cut into monoliths measuring 15 mm × 15 mm; these were used to assess the leaching of iodine, in accordance with an adaptation of the ANSI 16.1 testing methodology [37]. The ends of the sample cylinders were sealed with epoxy resin to allow only radial diffusion during leaching; upon drying of the resin, the monoliths were placed in contact with 47.1 mL of deionised water in sealed containers. Testing was completed in triplicate for monoliths and 'blanks' (leachate without cement monolith) in an environmental chamber at 20 °C to represent the average temperature for above ground ILW storage across the UK [38]. Sampling and total replacement of the leachate was completed at intervals of 2 and 7 h, then 1, 3, 7, 14, 21, 28 days, after which the containers were sealed. This methodology is an accelerated test that accentuates the alteration of the cement to provide a worst-case scenario of leaching characteristics from samples; in other words, the procedure depicts the potential for leaching in a much more aggressive environment than the real conditions of a storage/disposal facility. Immediately after sampling, the pH of the solutions was recorded; following, the liquid phases were stored in sealed containers at 20 °C until quantification of iodine through inductively couple plasma optimal emission spectroscopy (ICP-OES). After the leaching period had finished, the solids were dried, ground, and sieved below 63  $\mu m$  for characterisation through X-ray diffraction (XRD), thermogravimetry

**Table 4**Overview of the geopolymer samples prepared, highlighting the ID of the specimen, the adsorbent used, and the overall iodine uptake.

Sample ID	Adsorbent	lodine (mg/g)
GP <sup>·</sup> Ctrl	_	
GP _ <i>M1_Ag</i>	Mercaptosilica <sup>a</sup> + Ag	$1.1\pm2$
GP _ <i>M2_Ag</i>	MercaptoSil + Ag	$1.4 \pm 5$
GP _ <i>M2_Cu</i>	MercaptoSil + Cu	$0.6 \pm 5$
GP _T_Ag	TUPrSIL+ Ag	$2.3 \pm 5$
GP _T_Cu	TUPrSIL+ Cu	$1.2\pm 5$

<sup>&</sup>lt;sup>a</sup> Synthetised.

(TGA) and nuclear mass resonance spectroscopy (NMR).

The results were compared with preliminary tests conducted on the pure adsorbents exposed to alkaline conditions simulating the fresh geopolymer reaction mixture: 10 mg of pure adsorbent (without sorption of iodine) was added to 10 mL of activating solution (pH  $\sim$  15.2). This mixture was stirred using magnetic stirrer at room temperature for 2 h. The solution was then filtered using Whatman GF/C filter paper and washed twice with 10 mL of deionised water; finally, the filter paper was dried for 1 h at 80  $^{\circ}$ C and then weighed.

# 2.3. Characterisation techniques

Isothermal calorimetry (IC) was used to investigate the kinetics of reaction and phase formation during hydration/reaction of the wasteforms, and X-ray diffraction (XRD), Fourier transform infrared spectroscopy (FTIR), thermogravimetric analysis (TG), and solid state nuclear magnetic resonance (NMR) spectroscopy were used to characterize the hydration/reaction products. These techniques allowed for the determination of the local structure of the cements, and interaction of cement phases with adsorbents and/or potassium iodine. Details of each analytical approach are provided below.

IC data were obtained using dual channel TAM Air equipment from TA Instruments, with distilled water used as the reference. Cement pastes were hand mixed, and 20 g was placed into the glass testing ampoule; it was sealed and placed in the calorimeter at 20 °C for 7 days.

XRD was performed using a Panalytical X'Pert³, using CuK $\alpha$  radiation generated at 45 kV and 40 mA. Scans were run between 5 and 70° 2 $\theta$ , with a step size of 0.02° 2 $\theta$ , 2.2 s dwell per step, a LYNXEYE detector, an incident beam divergence of 1.0 mm and a 2.5° Soller slit in the diffracted beam, and the stage rotating at 15 rpm. Powdered samples were loaded onto 2.5 cm diameter and 1.0 mm deep sample holders. Qualitative phase identification was carried out using the Diffrac.EVA V4.1 software with the ICDD PDF4+ 2015 database.

FTIR data were obtained using a Perkin Elmer Frontier FTIR spectrometer equipped with a deuterated triglycine sulfate detector and KBr beam splitter optical system. The samples were prepared by blending together 2 mg of ground sample with 200 mg of KBr powder, i.e. KBr pressed pellet method; each specimen underwent 16 cycles of scanning at a resolution of 4 cm $^{-1}$  between 4000 and 400 cm $^{-1}$ . The contribution from atmospheric  $\rm CO_2$  and water vapour was removed by measuring the background prior to sample analysis.

Thermogravimetric analysis TGA was completed using a Perkin Elmer Pyris 1 TGA 4000, and the analysis was performed by considering 40 mg of powder. The samples were heated from 30 to 1000  $^{\circ}\text{C}$  in an alumina crucible at a rate of 10  $^{\circ}\text{C/min}$ , in a nitrogen atmosphere with a flow rate of 40 mL/min.

Samples for SEM-EDX analysis were mounted in epoxy resin and prepared for analysis by successive grinding using 600–4000 SiC grit papers before polishing on cashmere cloth coated with progressively finer (3  $\mu m-0.25~\mu m)$  diamond suspensions, with isopropanol as a lubricant. Data were collected using a Hitachi TM3030 SEM and a 15 kV accelerating voltage at a working distance of 8.5 to 9 mm. EDX was completed using a Bruker Quantax 70 detector and software to provide elemental maps that were collected for 600 s.

Solid-state NMR data were acquired on a Bruker Avance III HD 500 spectrometer at 11.7 T with a 4.0 mm dual resonance CP/MAS probe, producing Larmor frequencies of 99.35 MHz and 130.32 MHz for  $^{29}\mathrm{Si}$  and  $^{27}\mathrm{Al}$ , respectively. The  $^{29}\mathrm{Si}$  spectra were collected at a spinning speed of 12.5 kHz, with a minimum of 256 scans, a non-selective ( $\pi/2$ ) pulse width of 4  $\mu$ s, and a measured relaxation delay of 60 s.  $^{27}\mathrm{Al}$  spectra were collected at a spinning speed of 12.5 kHz, with a minimum of 512 scans, a selective ( $\pi/6$ ) pulse width of 1.7  $\mu$ s, and a measured relaxation delay of 5 s. The chemical shifts of the  $^{29}\mathrm{Si}$  and  $^{27}\mathrm{Al}$  nuclei were referenced to external samples of pure tetramethylsilane (TMS) and 1.0 M aqueous Al(NO<sub>3</sub>)<sub>3</sub> respectively. All data were processed using Bruker TopSpin 4.0.6 software.

ICP-OES analysis of the sampled leachate from the leaching tests was performed using a Spectro Ciros Vision Inductively Coupled Plasma-Optical Emission Spectrometer, operated using a gold internal standard and ceramic torch. Samples were filtered (0.22  $\mu m)$ , diluted and acidified with 20  $\mu L$  of concentrated HNO3 (99.999 % purity) prior to analysis. Calibration curves were prepared by measuring intensities against a series of known calibration standards, which were prepared by diluting single element standard solutions (Fisher Scientific) with 1 % (v/v) HNO3.

# 3. Results and discussion

#### 3.1. Adsorbent loading

#### 3.1.1. Hydration and reaction kinetics

After curing for 28 days, all the BFS:PC and geopolymer samples had fully set, and were demoulded from the sample containers. Here, the hydration kinetic of the BFS:PC and PC samples is discussed by considering the IC data displayed in Fig. 3A and B, respectively.

The hydration mechanism of BFS in the presence of PC have already been extensively investigated [32], with the reaction kinetics of blended PC and BFS being lower than that of PC only. Specifically, the hydration

in the BFS:PC control sample can be divided into several consecutive steps: pre-induction, induction, acceleration, deceleration, and steady-state periods. The pre-induction, induction, and acceleration steps are important since they allow for initial mixability, pumpability time, and development of the early strength of the paste. At this stage, the main hydrated species ettringite (AFt), calcium silicate hydrate (C-S-H), and portlandite (Ca(OH)2) precipitate upon reaction between alite (C3S), belite (C2S), aluminates, gypsum, and water. However, it is well known that the hydration rate of PC is decreased by the presence of supplementary cementitious materials (SCMs), such as BFS; in fact, the dissolution of the BFS only starts to occur in alkaline conditions, i.e. when the precipitation of portlandite Ca(OH)2 from the hydration of PC starts, via pozzolanic reaction [33].

The introduction of adsorbents to the fresh cement paste appeared to retard the hydration kinetics of BFS:PC samples, as shown in Fig. 3A. The precipitation of Ca(OH)<sub>2</sub>, occurring between 1 and 10 h [33], was observed as a sharp heat evolution peak with a maximum at approximately 5 h for the reference sample BFS:PC\_Ctrl (Fig. 3A). Retardation of the hydration kinetics in samples containing adsorbents is likely to arise from retardation of precipitation of Ca(OH)<sub>2</sub> in these samples. Likely, the reaction between the  $Ca_{(aq)}^{2+}$  and the non-metalated silicate chains of the adsorbents led to a lower availability of  $Ca^{2+}$  ions in solution,

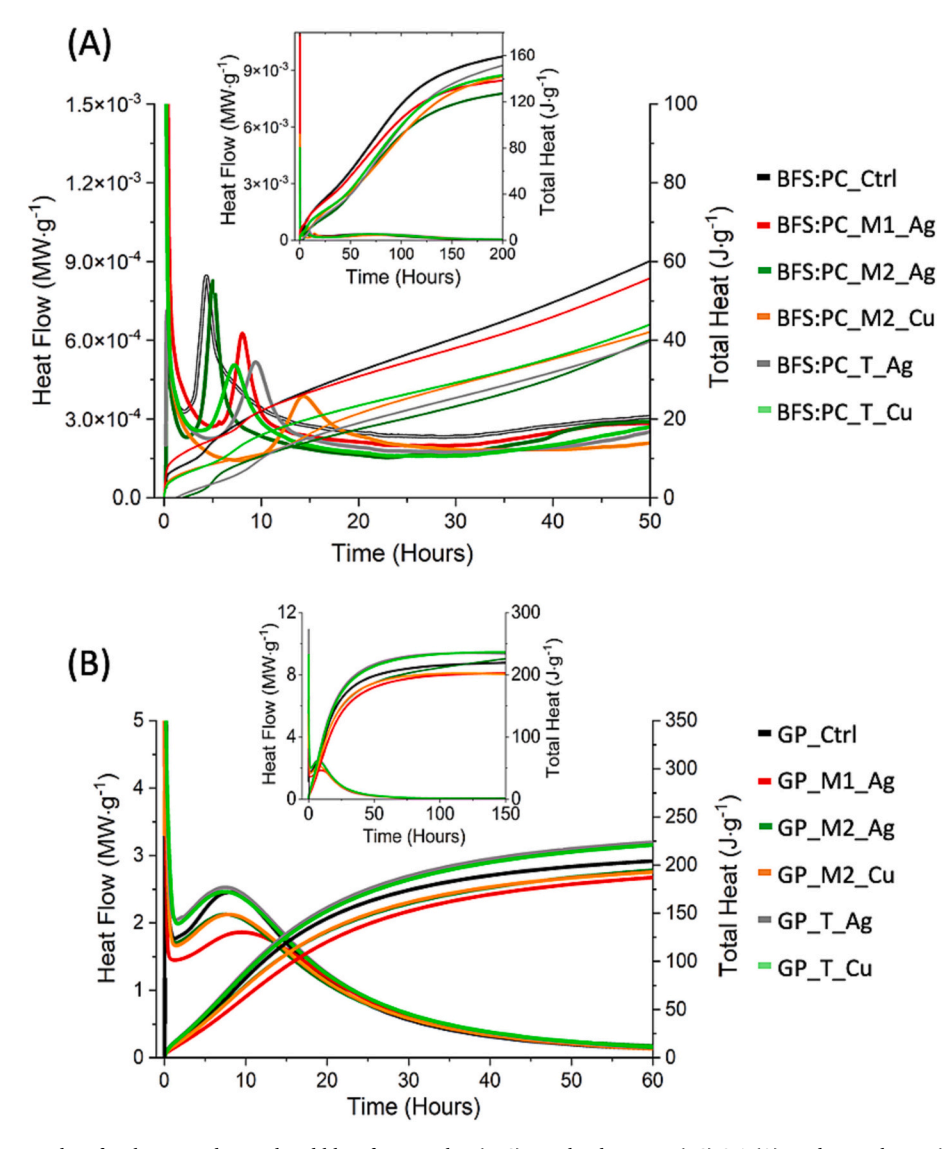


Fig. 3. Isothermal calorimetry data for the ground granulated blast furnace slag (BFS)/Portland cement (PC) 3:1 (A), and geopolymer (B) wasteforms. Samples are identified in the legend as described in Table 3 and Table 4.

increasing the time required to reach the supersaturation conditions required for the precipitation of portlandite, and therefore the dissolution of BFS in these cements. Furthermore, some metalated ligands on the adsorbents might undergo events of metal substitution between  ${\rm Ag}^+/{\rm Cu}^{2+}$  and  ${\rm Ca}^{2+}$  ions in the pore solution, upon charge balancing. In this case, a lower availability of  ${\rm Ca}^{2+}$  ions within the pore solution would occur, retarding the precipitation of  ${\rm Ca}({\rm OH})_2$  and therefore the overall hydration rate.

One of the samples with the least affected hydration reactions (c.f. the control sample) was for BFS:PC\_M2\_Ag, which was noticeably different to the synthesised BFS:PC\_M1\_Ag. The same type of Ag-loaded adsorbent (synthetized mercaptosilica) led to a 3-h longer induction period in BFS:PC\_M2\_Ag compared with the commercially purchased BFS:PC\_M1\_Ag. The incorporation of Cu-loaded MercaptoSil in BFS:PC\_M2\_Cu led to a 10-h retardation with respect to BFS:PC\_M2\_Ag, therefore suggesting that the hydration kinetics would be hindered when copper is used for resin metalation. However, T\_Cu in BFS:PC\_T\_Cu was showing a 3-h shorter induction period when compared to T\_Ag in BFS:PC\_T\_Ag, suggesting that the relationship between the metal-ligand-silica system and the reaction kinetics during hydration of the PC:BFS wasteforms is not trivial.

Despite their complexity, the trends observed for these samples are consistent with the mechanism proposed above, suggesting that the slower hydration kinetics are a result of substitution of the adsorbent bound metal ions Ag<sup>+</sup> or Cu<sup>2+</sup> with the Ca<sup>2+</sup> ions within the pore solution. The different extent of retardation of the hydration of the BFS:PC wasteforms appears to be dependent on the adsorbent encapsulated, and is likely to arise from differing strengths of the bonding interactions between the metal and the ligand in each type of adsorbent; in this case, the stability of the T\_Cu complex was higher than the T\_Ag one, and vice versa for M2. Such an observation is corroborated by the affinities of the two metals studied for each ligand, since the bond strength between Ag+ and M2 is stronger than Cu2+ and M2, as reflected by the respective absolute association constants  $\beta$  of 4.07  $\times$  10<sup>10</sup> and 1.26  $\times$  10<sup>11</sup>. Similarly, the weaker binding strength expected for  $\mbox{Ag}^{+}$  and T (K  $\sim\!10^{13}$ [34]) with respect to  $\text{Cu}^{2+}$  and T (K  $\sim 10^{10}$  [35]) was in line with the retardation of the hydration observed when the complex Cu<sup>2+</sup>/T was considered. However, further investigation is required to isolate and assess the effects of different metal ligands on hydration kinetics, since the reaction rate might influence the structure and stability of the resulting material. Clearly, the synthetic differences between BFS: PC\_M1\_Ag and BFS:PC\_M2\_Ag are influencing hydration kinetics and it is proposed that the variation in porosity in the silica might explain the observed behaviour. Despite the differences in the hydration kinetics observed, all the BFS samples analysed here underwent final set within 24 h by not exceeding the 180 kJ kg<sup>-1</sup> heat released (Fig. 3A), within the limits set by Sellafield Ltd. for cement used as wasteform. The control sample was exhibiting the most exothermic reaction among the samples considered here.

IC data for the geopolymer samples (Fig. 3B) encapsulating the adsorbents did not differ significantly from that of the control sample GP\_Ctrl. The geopolymerisation process firstly involves the alkaline dissolution of the aluminosilicate sources into aluminate and silicate monomers, reflected by the first exothermic peak occurring within minutes. It is followed by another exothermic reaction involving the proper breakdown of the silica chains of the MK to produce alumina/silicahydroxy species and oligomers, such as OSi(OH)<sub>3</sub>, Al(OH)<sub>4</sub>, (OH)<sub>3</sub>-Si-O-Al-(OH)<sub>3</sub>. Following this, the exothermic peak observed up to 60 h of curing results due to the progression of those polymerisation reactions leading to the hardening of the paste [36]. As expected, the maximum heat flow value was registered between 8 and 10 h of curing, with the adsorbents apparently not influencing any of the characteristic reaction steps, i.e. initial dissolution (<1 h), induction period (1-2 h) and polymerisation (>2 h), of the geopolymerisation (Fig. 3B). Only M1\_Ag exhibited a slight retardation, with the maximum heat flow value detected just above 10 h of curing. However, the different adsorbents led

to a varying cumulative heat release after 150 h of curing, the highest for which was for the materials with T as the ligand. The heat release from the control sample exceeded 200 J g $^{-1}$  after 150 h of curing, slightly higher than the remaining samples GP\_M1\_Ag, GP\_M2\_Ag and GP\_M2\_Cu. Likely, the lower heat generation observed for the adsorbent containing samples is a result of the adsorbent behaving like secondary mineral phases within the metakaolin product, diluting the thermal output of the reaction. Although this is not significant at the current levels of loading, it will be of interest for increased loading of adsorbents into the systems. Despite the higher cumulative heat release, with respect to the BFS:PC (Fig. 3A), these outcomes suggested that the geopolymer systems considered were also below the maximum heat release requirements for cement use as a wasteform by standards used at Sellafield Ltd., i.e. <180 kJ kg $^{-1}$  released in the first 24 h.

# 3.1.2. Phase assemblage

The XRD analysis of the BFS:PC samples hydration products (Fig. 4A) confirmed the presence of ettringite (Powder Diffraction File, PDF, 00-041-1451), monocarboaluminate (PDF 00-036-0377), a hydrotalcitelike phase (PDF 00-014-0525), portlandite (PDF 00-044-1481), and calcium aluminosilicate hydrate with a tobermorite-like configuration (PDF 00-034-0002). Minor reflections for calcite (PDF 00-005-0586) and unreacted belite (PDF 00-023-1044) were also detected. The XRD patterns reported in Fig. 4A suggested that inclusion of different adsorbents did not affect the type of phases formed when compared to the control sample. The data from thermogravimetric analysis (Fig. 4B) supported the XRD data, registering total loss on ignition (LOI) values around 10-11 mass% for all the samples. The loss of water from the main hydrated species Aft/AFm [37], C-A-S-H [38], and Ht [39] was observed between 30 and 200 °C, amounting to around 6 mass% both for the control and adsorbent loaded samples. That suggested a similar hydration extent achieved from all the samples after 28 days of curing, regardless of the adsorbent. The gradual weight loss observed between 270 and 470 °C, overlapping with the de-hydroxylation of portlandite occurring between 400 and 500 °C [40], is proposed to be the result of further thermal decomposition of hydrotalcite [39].

The endothermic peak linked to the de-hydroxylation of portlandite was not observed in BFS:PC\_M2\_Ag and BFS:PC\_M2\_Cu, potentially suggesting that Ag could hinder the precipitation of portlandite; on the contrary, the Ag-loaded adsorbent M1\_Ag led to the precipitation of portlandite. As discussed above, this difference might result from differencing strengths of the bonding interaction between Ag and the specific adsorbent, with the data here suggesting a stronger Ag-ligand bonding interaction for M1 rather than M2, where some of the Ca<sup>2+</sup> ions could replace some Ag+ upon charge balancing. Potentially, the lower weight loss observed between 400 and 450 °C for the adsorbent containing blends may indicate pozzolanic reaction of the adsorbents had initiated. Finally, the release of CO<sub>2</sub> from residual CaCO<sub>3</sub> was likely identifying the weight losses observed between 600 and 750 °C, whereas the decarbonisation detected around 900 °C could not be attributed with certainty. Likely, it was referring to the further loss of CO<sub>2</sub> from CaCO<sub>3</sub> crystals trapped in the double layers during the de-hydroxylation of AFm, AFt, and Ht. Their complex thermal degradation might result in a re-arrangement of the solids upon heating, leading to the trapping of CaCO<sub>3</sub> crystals within the re-arranged structure.

Regarding the geopolymer samples, the XRD analysis (Fig. 4A) did not show any detectable difference between the control and the adsorbent containing samples, with the only identifiable crystalline phases arising from those in the metakaolin precursor, including rutile (TiO<sub>2</sub>, PDF 01-084-0286), kaolinite (Al<sub>2</sub>O<sub>3</sub>·2SiO<sub>2</sub>·2H<sub>2</sub>O, PDF 75-1593), and quartz (SiO<sub>2</sub>, PDF 46-1045) (Fig. 5).

Diffuse scattering between 22 and  $36^{\circ}$  20 is consistent with the presence of an amorphous potassium aluminosilicate hydrated (K)-A-S-H gel phase, and no additional phases were observed via XRD to form upon addition of adsorbents and iodine. The TG analysis (Fig. 5B) also indicated very high similarity between all the geopolymer systems

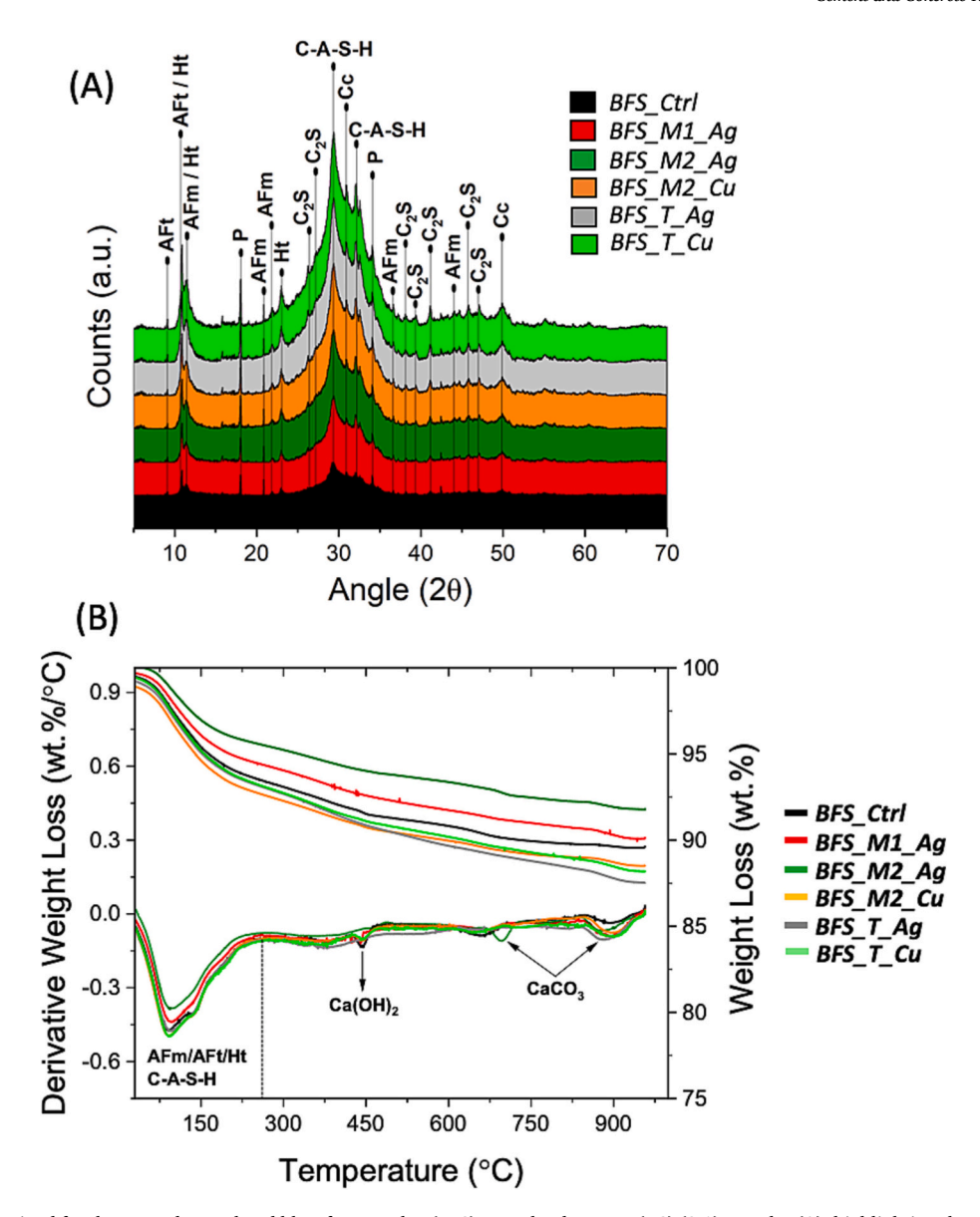


Fig. 4. XRD patterns obtained for the ground granulated blast furnace slag (BFS) / Portland cement (PC) (3:1) samples (A), highlighting the peaks for ettringite (AFt), monocarboaluminate (AFm), Hydrotalcite (Ht), Portlandite (P), C-A-S-H gel, calcite (Cc), and larnite (C2S). Thermogravimetric analysis conducted on the BFS:PC samples, highlighting the main weight losses events (B).

investigated, including the control one; indeed, all these samples were showing the same signal between 30 and 300 °C, accounting for a 13.7 mass% weight loss, on average. Such a signal was composed of two overlapping peaks, and therefore they could not be resolved independently. The intensity was in line with other data in literature [41], and arises due to the release of free and/or slightly bound water present in the samples. Considering that mean LOI values of 16.7 mass% were registered throughout the temperature ramp, the signal below 300 °C was representing the near totality (~82.3 mass%) of the total weight loss observed. The following weight loss observed between 350 and 700  $^{\circ}\text{C}$ (2.0 mass% on average) was likely referring to the dehydroxylation of the geopolymer matrix, the removal of the surface hydroxyl groups, and the formation of Si-O-Si bonds leading to the release of water and the shrinkage of the overall structure [42]. The remaining weight loss observed up to 800 °C, 1.0 mass% on average, was likely referring to a further water release from the system [43].

#### 3.1.3. Nanostructure

The nanostructure of all the samples was investigated through NMR

 $(^{29}\text{Si},^{27}\text{Al})$  and FTIR analyses. For all the BFS:PC samples, the  $^{29}\text{Si}$  MAS NMR data (Fig. 6A) comprise four overlapping resonances with maximums at  $\delta_{iso} = -74$  ppm  $(Q^0), -75$  ppm  $(Q^1(1\text{Al})), -79.0$  ppm  $(Q^1)$  and -81.6 ppm  $(Q^2(1\text{Al})), -84.4$  ppm  $(Q^2)$  [44].

These resonances are attributed to  $Q^0$  sites within unreacted BFS particles, and  $Q^1(1Al)$ ,  $Q^1$ ,  $Q^2(1Al)$ , and  $Q^2$  sites within an aluminium-substituted calcium silicate hydrate (C-A-S-H) gel, typical of that formed in hydrated BFS:PC wasteforms [45]. Whereas, a single broad resonance of the  $Q^n(mAl)$  environments (maximum intensity at  $\delta_{iso} = -75$  ppm), characterised by a lower polymerisation or higher Al substitution, refers to the presence of anhydrous slag [46]. Only slight variations could be detected with respect to the control sample, probably linked to the shorter length of the silicate chains (fewer  $Q^2$  positions) in the C-(A)-S-H; the lack of variation of the resonance attributed to  $Q^0$  sites was also justifying it. The  $^{27}$ Al data (Fig. 6C) confirmed the high similarity of all the BFS:PC samples, as outlined above. The broad tetrahedral Al resonance with maximum at  $\delta_{iso} = 63$  ppm could be attributed to the multiple overlapping AlO<sub>4</sub> sites including Al in bridging tetrahedra and Al in crosslinked bridging tetrahedra ( $q^3$ ) within the

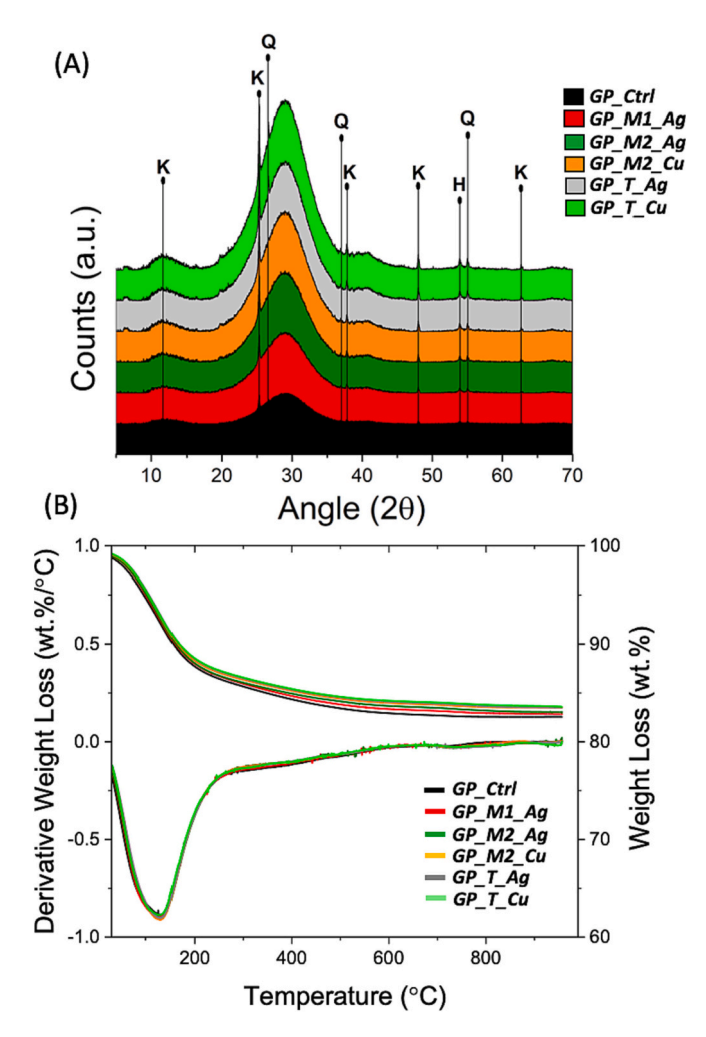


**Fig. 5.** XRD patterns obtained for the geopolymer samples (A), highlighting the peaks for rutile, kaolinite, and quartz. Thermogravimetric analysis conducted on the geopolymer samples, highlighting the main weight losses events.

aluminosilicate chains in the C-A-S-H gels [47], as well as Al in unreacted slag particles. The resonances at 11 ppm and 13 ppm also support the XRD analysis, and are due to  $AlO_6$  sites in AFm-type phases (e.g. mono- and hemicarboaluminate) and ettringite, respectively (octahedrally coordinated Al(VI)) [47].

Regarding all the GP samples, the <sup>29</sup>Si MAS NMR data (Fig. 6B) exhibit a broad resonance spanning from  $\delta_{\text{iso}} = -70$  ppm to -110 ppm, with a consistent line shape and a maximum at  $\delta_{iso} = -87.8$  ppm, also suggesting slight differences in upon adsorbent loading. Such resonance is attributed to a distribution of Q<sup>4</sup>(mAl) local sites within K-A-S-H [48] (where 0 < m < 4), confirming the alkali activation of the metakaolin, whose original signals [49] are replaced by  $Q^4(4Al)$  and  $Q^4(3Al)$  sites. The line shape and position of the chemical shift distribution for all geopolymer samples analysed here is very similar to that observed previously by deconvolution and quantification of <sup>29</sup>Si MAS and <sup>1</sup>H-<sup>29</sup>Si CPMAS NMR data for similar geopolymer cements, and indicate the formation of an Al-rich (Si/Al  $\leq$  1.2) K-A-S-H gel with similar chemical composition, comprising Q<sup>4</sup>(4Al), Q<sup>4</sup>(3Al) and Q<sup>4</sup>(2Al) sites. As expected, also the <sup>27</sup>Al MAS NMR data (Fig. 6D) could not outline any detectable changes in the nanostructure of the GP samples upon adsorbent loading, therefore suggesting that no changes have occurred in the local Si surroundings within the (N,K)-A-S-H gels. The nearly complete dissolution of metakaolin is confirmed by the weak intensity of the characteristic resonances at  $\delta_{\text{obs}} = 33$  and 8 ppm [50], while the resonance at  $\delta_{obs} = 56$  ppm was overlapping with the main resonance detectable between  $\delta_{obs}=50$  and 70 ppm. This resonance exhibited a maximum centred at  $\delta_{obs}=60.7$  ppm and is attributed to tetrahedral AlO<sub>4</sub> sites within the K-A-S-H gel [51] (Fig. 6D).

To further investigate nano-scale variations that may have occurred due to encapsulation of the adsorbent/iodine complexes within the geopolymer cements, FTIR spectroscopy was performed on the samples prepared with Mercaptosil-Ag and Cu, since they reported the highest (BFS:PC M2 Ag) and lowest (BFS:PC M2 Cu) hydration kinetics in the BFS:PC system (Fig. 3A). The FTIR data for the BFS:PC and GP samples, reported as supplementary electronic material (SEI-I), confirmed the absence of any changes in the nanostructure of all the samples produced upon adsorbent loading. The nearly complete dissolution of BFS was observed at 28 days of curing, with the typical signals at  $\lambda = 1021 \text{ cm}^{-1}$ [52] replaced by the characteristic peaks of C-A-S-H around 960 cm<sup>-1</sup>, referring to the asymmetrical stretching vibrations ( $\nu_{as}$  Si-O-Si) of the Si—O bonds [53]. The diffused signals referring to the presence of water, between 1400 and 3700 cm<sup>-1</sup> and with maxima at 3498, 1662 and 1494 cm<sup>-1</sup>, suggested the presence of a poorly crystalline phase or constrained water, and therefore confirming the presence of hydrated aluminosilicates [54]. The FTIR analysis performed on the GP samples loaded with the same adsorbents is also reported in SEI—I; in accordance with the previous discussion, the advanced reaction extent of metakaolin at 28 days of curing was reflected by the hidden signal around 1060 cm<sup>-1</sup>, usually referring to the asymmetric stretching of the Si-O-T chains [55]. The main overlapping signal registered at 993 cm<sup>-1</sup> refers to the resonance of K-A-S-H gel; the shift to lower wavelength, with respect to unreacted metakaolin, suggested a higher percentage of Si-O-Al bridging interactions. In fact, while unreacted metakaolin is predominantly consisting of Q<sup>4</sup>(1Al) local sites, with a single silicon atom tetrahedrally coordinated with four atomic centres (of which 3 silicon and 1 aluminium atom) [56], a shift to a highly Al substituted local structure was observed for the alkali activated solid. In fact, the distribution of the Si-O-T linkages changes towards the predominant presence of  $Q^4(4Al)$  and  $Q^{4(3Al)}$  sites (Fig. SEI I) [48].

#### 3.2. Leaching tests

The pH of all the solutions sampled after the targeted leaching periods was registered, and the trends for the BFS:PC and GP samples are reported in Fig. 7A and B, respectively; as reported in the experimental section, the leaching medium was replaced with fresh one after each sampling, and therefore the value registered refers to the timeframe highlighted.

Both the BFS:PC and GP led to an increase of pH with respect to the blank (7.0  $\pm$  0.8), due to the dissolution of Ca(OH)<sub>2</sub> [57] and alkali in the former and latter, respectively. While the dissolution extent of Ca (OH)<sub>2</sub> in the BFS:PC samples appeared to decrease beyond 7 days, reflected by a pH drop from  $10.2 \pm 0.3$  to  $8.7 \pm 0.5$ , a constant alkalinity (pH of  $11.5 \pm 0.5$ ) was observed for all the GP samples for the first 7 days of leaching, after which the pH decreased to between pH 11.0 and pH 9.5, depending on the adsorbent encapsulated. The partial dissolution of the solids suggested by the pH trends was further confirmed by the detection of Si in the liquid phase, whose trends are reported in SEI-II both for the BFS:PC and GP samples. In the GP leachates, the Si concentration increases up to 150 days, but then decreases to significantly lower values, suggesting formation of a secondary phase containing Si. However, there is no clear evidence of this Si-containing phase in the SEM micrographs obtained for the samples after leaching. The SEM micrographs of the control GP and BFS:PC monoliths cured in deionised water up to 28 days is reported in Fig. 8A and B below, respectively, with highlight on the textural properties of the surface.

While no apparent modifications could be detected for the GP sample both in the inner and outer regions (Fig. 8A), showing homogeneity at any depth from the boundaries, distinct local regions were outlined for the BFS:PC sample (Fig. 8B). The texture was denser at the level of the solid bulk (region 1), whereas the contact with water led to a higher

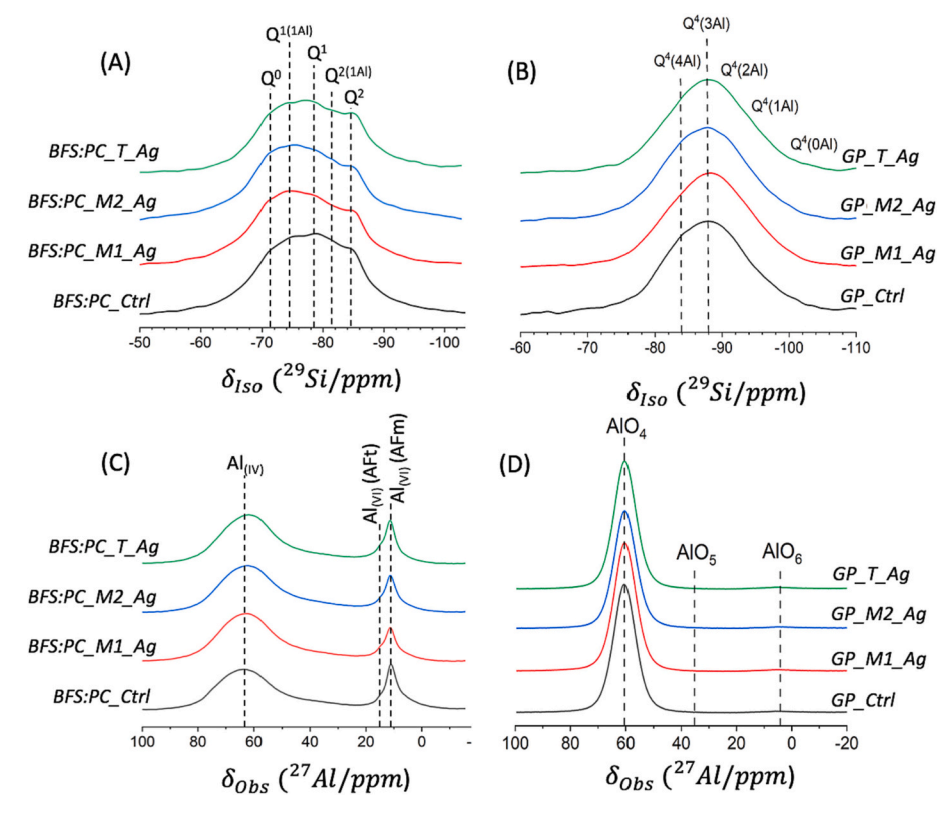


**Fig. 6.** <sup>29</sup>Si (A) and <sup>27</sup>Al (C) MAS NMR data for the ground granulated blast furnace slag BFS / Portland cement PC samples with Ag-containing adsorbents (M1\_Ag, M2\_Ag, T\_Ag) at 28 days, with respect to the control sample. <sup>29</sup>Si (B) and <sup>27</sup>Al (D) MAS NMR data for the geopolymer samples with Ag-containing adsorbents (M1\_Ag, M2\_Ag, and T\_Ag) at 28 days, with respect to the control sample.

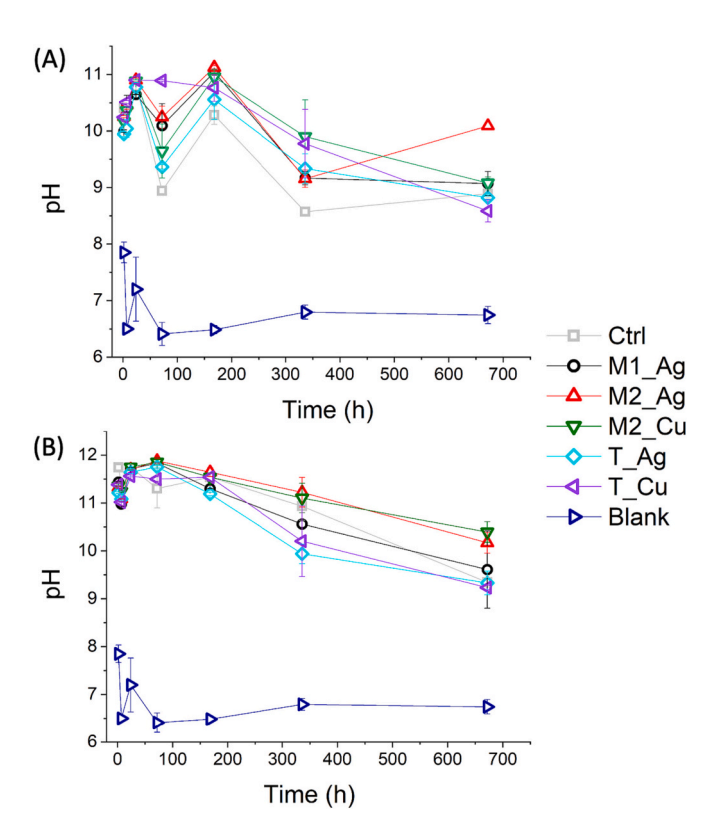


Fig. 7. Average pH of samples at each testing point for BFS:PC (A) and GP (B) samples.

porosity in proximity of the solid/liquid interface (region 2); such an observation was based on the increased portion of voids (dark grey) with respect to the solid bulk. Furthermore, some non-continuous deposits of precipitated solids could be observed at the solid/liquid interface (region 3); likely, such precipitates were referring to calcite particles resulting from the availability of  $Ca^{2+}$  and  $CO_3^{2-}$  ions within the leachate and the achievement of the supersaturation conditions. The partial dissolution of Ca(OH)<sub>2</sub> could have provided the Ca<sup>2+</sup> ions into the liquid bulk, whereas the  $CO_3^{2-}$  ions were likely a result of dissolution of a small amount of atmospheric CO2 during sample handling and preparation. Despite these outcomes would confirm the partial dissolution of the monoliths, the degradation of the adsorbents could only be assessed via detection of iodine through ICP-OES analysis of the liquid phases. The rate k (mg s<sup>-1</sup>) of leaching iodine could be calculated through Eq. 2 below, where the terms  $I_f$ ,  $V_L$ , and  $\Delta t$  reflect the final concentration of iodine within the leachate (mg L<sup>-1</sup>), the volume of the leachate (L), and the time interval (s), respectively; the outcomes are reported in Fig. 9A and B for the BFS:PC and GP samples, respectively.

$$k = I_f \bullet V_L/_{\Delta f} \tag{2}$$

As reported, the iodine leaching rate for the geopolymer samples was approximately 1.5 orders higher than the BFS:PC ones throughout the time intervals considered; specifically for the three-days tests, average leaching rates of  $2.9 \cdot 10^{-5}$  and  $1.2 \cdot 10^{-6}$  mg<sub>Iodine</sub> per second were calculated, respectively. However, both the systems were undergoing a rapid drop beyond that, until nearly stationary conditions were achieved after 14 days. That could be due to 1) a slower progression of the leaching front within the monoliths, or 2) that iodine quantitatively leached out of both the systems. To assess this, the cumulative iodine release  $\nu_I$ , expressed as a fraction of the total iodine initially inserted, was calculated by considering the original loading of iodine reported in Table 5.

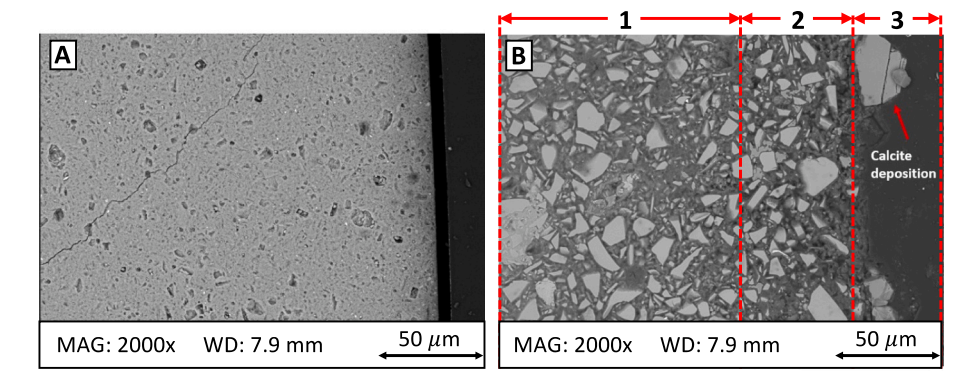
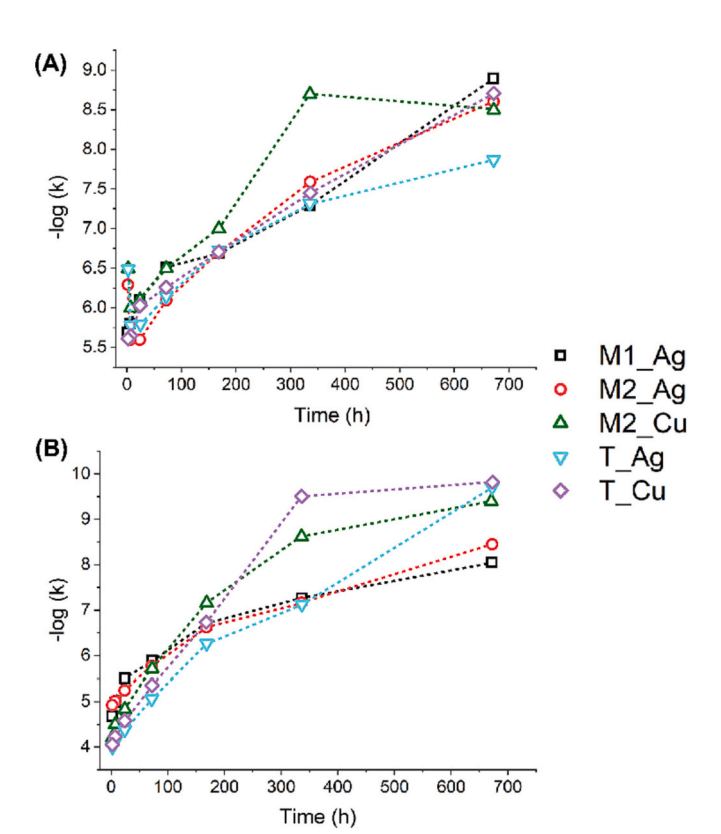


Fig. 8. SEM Micrographs of the GP\_Ctrl (A) and BFS:PC\_Ctrl (B), demonstrating the microstructural changes resulting from leaching of the samples.



**Fig. 9.** Leaching rate of iodine, expressed in mg·s<sup>-1</sup>, reported in -log scale for a better visibility of the results regarding the BFS:PC (A) and GP (B) samples.

Table 5 Overview of the iodine content within each samples monolith considered, together with the theoretical iodine concentration in the leachate  $(47.1\ mL)$  assuming a complete dissolution.

Sample ID	Iodine (mg $g_{cement}^{-1}$ )	$I_{Th}$ (mg $L^{-1}$ )
BFS:PC_M1_Ag	4.6	96.8
BFS:PC_M2_Ag	5.6	119.3
BFS:PC_M2_Cu	2.5	53.9
BFS:PC_T_Ag	3.9	196.6
BFS:PC_T_Cu	4.1	104.0
GP_M1_Ag	3.9	83.6
GP_M2_Ag	5.1	107.6
GP_M2_Cu	2.2	46.5
GP_T_Ag	8.5	180.5
GP_T_Cu	4.3	92.4

Assuming a total release of iodine, the theoretical concentration  $I_{Th}$  within the known volume of leachate (47.1 mL) could be calculated. Subsequently, starting from the punctual iodine concentration  $\nu_{I,n}$  detected at a given time interval  $\Delta t_n$  ( $n=2\,h,7\,h,24\,h,3d,7d,14d,28d)$  the total fraction of leached iodine  $\nu_{I,f}$  could be calculated through Eq. 3 below.

$$\nu_{l,f} = \frac{\sum_{2h}^{28d} \nu_{l,n}}{I_{Th}} \tag{3}$$

The fraction of leached iodine  $\nu_{I,n}$  is plotted in Fig. 10A and B for all the BFS:PC and GP samples, respectively; a complete overview of all the samples here discussed is reported in Table 6 below, where the effective diffusivity is also considered.

As reported in Fig. 9A, the BFS:PC wasteform allowed for a relatively small fraction of iodine to leach out; in fact, independently from the adsorbent used, a maximum iodine fraction  $\nu_{I,f}$  of 0.08 was leached after 28 days. Likely, the iodine-loaded adsorbents would not degrade at the

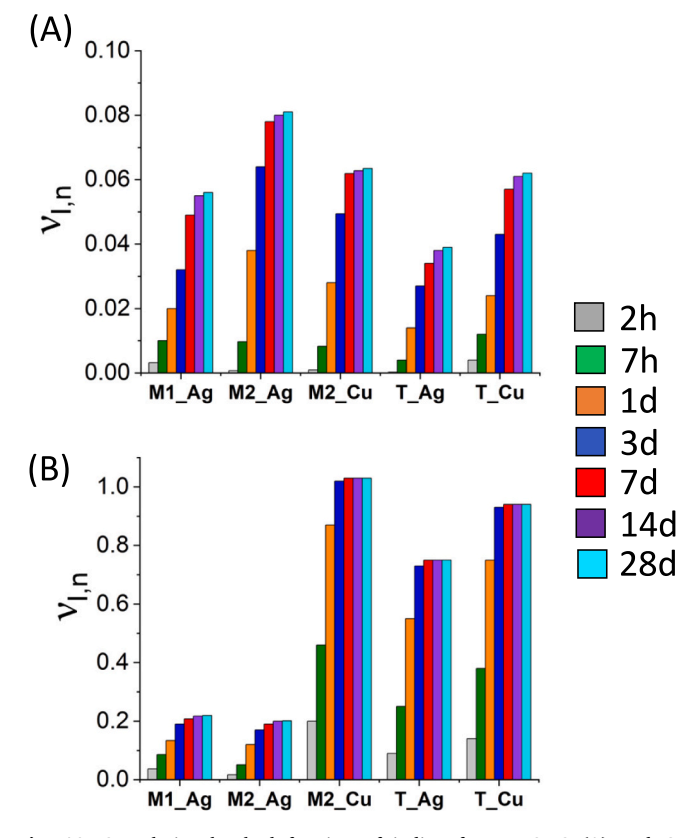


Fig. 10. Cumulative leached fraction of iodine from BFS:PC (A) and GP (B) samples.

Table 6

Total released iodine from leached cement samples and average effective diffusivities.

Adsorbent reference	Total released I		Average effective diffusivity (cm <sup>2</sup> /s)	
	BFS:PC	GP	BFS:PC	GP
M1_Ag	6	22	$3.7\times10^{-10}$	$1.4 \times 10^{-8}$
M2_Ag	8	20	$1.5 \times 10^{-9}$	$1.1\times10^{-8}$
M2_Cu	6	103	$1.2 \times 10^{-9}$	$6.1 \times 10^{-7}$
T_Ag	4	75	$2.2 \times 10^{-10}$	$2.1 \times 10^{-7}$
T_Cu	6	94	$6.1 \times 10^{-10}$	$4.8 \times 10^{-7}$

alkaline conditions within the BFS:PC samples, and iodine would be withheld in the insoluble adsorbent material. In other words, the adsorbents would not degrade upon interaction with the cementitious matrix; therefore, the iodine-loaded adsorbents would physically migrate towards the leachate, but a low dispersion of iodine would occur. However, the detection of iodine allowed for the calculation of the effective diffusivities within the BFS:PC samples [58], which ranged between  $3 \times 10^{-13}$  and  $7 \times 10^{-9}$  cm<sup>2</sup>·s<sup>-1</sup> (Table 6); such values were lower than other studies introducing 1 wt% silver zeolite into a similar blended PC system [59]. This is likely a result of both the ligand-metal-iodine interaction slowing iodine release, as well as the porosity differences between the silica materials and the silver zeolite [15,27]. Regarding the GP samples (Fig. 9B), a higher fraction of iodine would leach out with respect to the BFS:PC ones, and it was clear that different adsorbents led to varying leaching extents. Generally, the systems with Ag-loaded adsorbents were retaining more iodine that those with Cu, for which the iodine leaching was nearly quantitative; however, both cases led to a failure of the system to retain iodine, given the likely degradation of the adsorbents due to the very high internal pH. Such data seemed to confirm the degradation of the adsorbents, despite the fact that ICP-OES detection of Ag and Cu was beyond the limits of the analysis. A good correlation between the effective diffusivities reported in Table 6 (4  $\times$  10<sup>-12</sup> - 1.5  $\times$  10<sup>-6</sup> cm<sup>2</sup>·s<sup>-1</sup>) and the literature investigating the leaching of Cs from PC was found [60]. When looking at the trends in Figs. 7B and 10B, it is notable that the highest recorded iodine concentrations do not match with the highest recorded pH, which were buffered to high values until 7 days. Furthermore, I, Ag, and Cu are redox-sensitive elements, and will exhibit different speciation in different redox conditions present in the each wasteform type. BFS dissolution during wasteform formation will result in reducing conditions in the BFS:PC wasteform, where Ag and I are expected to be present as Ag<sup>0</sup> and I<sup>-</sup>., whereas the oxic conditions present in the GP wasteforms means Ag and I are expected to be present as  $Ag^+$  and  $IO_3^-$  [61–63]. The redox conditions present would therefore also contribute to the differences in leaching seen between each wasteform type.

# 4. Conclusions

This study investigated BFS:PC and geopolymer cement wasteforms encapsulating three different hybrid silica adsorbents, chosen based on previously published work identifying optimum iodine uptake in the order of 100–150 mg per gram of adsorbent: in-house synthetized Mercaptsosilica, commercially available MercaptoSil, and commercially available TUPrSILA.

 Encapsulation of the adsorbents resulted in the retardation of the hydration reaction for the BFS:PC wasteforms. This is attributed to the reaction between the Ca<sup>2+</sup><sub>(aq)</sub> and the non-metalated silicate chains of the adsorbents leading to a lower availability of Ca<sup>2+</sup> ions in solution, increasing the time required to reach the supersaturation conditions required for the precipitation of portlandite, and therefore the dissolution of BFS in these cements.

- Encapsulation of the adsorbents in the geopolymer wasteforms resulted in negligible effects on the reaction kinetics during wasteform formation
- All BFS:PC samples were in accordance with the current Sellafield requirements in terms of total evolved heat and estimated set time, whereas the geopolymer ones slightly exceeded them whilst in line with the data from the literature [64].
- No phase assemblage nor microstructural changes could be detected for any of the BFS and geopolymer samples upon addition of the iodine-adsorbent complexes.
- The GP wasteform did not show any observable chemical or microstructural changes after leaching, whereas a significant alteration layer was observed near the surface of the BFS:PC wasteform after leaching, with different chemical composition and microstructure than the bulk.
- The leaching experiments showed that that, despite the above point, BFS:PC wasteforms exhibited better iodine retention than GP wasteforms, most likely because of degradation of the adsorbent in the very high pH of the fresh GP reaction mixture.
- Different iodine leaching extents were observed for the different adsorbents loaded on the GP system, suggesting potential for further investigation into other types of adsorbents.

The further investigation on the breakdown of the adsorbents and resulting distribution of the functional groups / iodide is required to achieve acceptable performances in terms of iodine retention, likely adjusting the overall alkalinity of the GP matrix and therefore acting on the basic formulation used. In addition, durability testing that enables comparison to other iodine wasteform concepts is important to enable decision making on the best concept for iodine capture and disposal. Overall, this work evidences the potential for cement-based wasteforms to encapsulate radioiodine-loaded adsorbents if it can be shown that iodine retention is sufficient for disposal conditions. Therefore, this work contributes to a potential "Near Zero" discharge policy and highlights the importance of synergy in design and implementation of adsorbent materials and the final wasteform to be used for radioiodine abatement.

# CRediT authorship contribution statement

Marco Simoni: Data curation, Formal analysis, Investigation, Writing – original draft. Sarah A. Kearney: Data curation, Formal analysis, Investigation, Methodology, Writing – original draft. Thomas J. Robshaw: Data curation, Formal analysis, Investigation, Methodology, Writing – original draft. Joshua Turner: Conceptualization, Project administration, Supervision, Validation, Writing – review & editing. Kyle O'Donoghue: Data curation, Formal analysis, Investigation, Methodology, Writing – original draft. Daniel A. Geddes: Data curation, Formal analysis, Investigation, Methodology. Clint A. Sharrad: Funding acquisition, Project administration, Supervision, Writing – review & editing. Mark D. Ogden: Conceptualization, Funding acquisition, Project administration, Data curation, Formal analysis, Funding acquisition, Investigation, Methodology, Project administration, Resources, Supervision, Writing – review & editing.

# **Declaration of competing interest**

The authors declare the following financial interests/personal relationships which may be considered as potential competing interests: Brant Walkley reports financial support was provided by United Kingdom Department for Business Energy and Industrial Strategy. Mark D. Ogden reports financial support was provided by United Kingdom Department for Business Energy and Industrial Strategy. Clint A. Sharrad reports financial support was provided by United Kingdom Department for Business Energy and Industrial Strategy.

#### Data availability

Data will be made available on request.

#### Acknowledgements

This work was funded by the under the £46m Advanced Fuel Cycle Programme as part of the Department for Business, Energy and Industrial Strategy's (BEIS) £505m Energy Innovation Programme.

# Appendix A. Supplementary data

Supplementary data to this article can be found online at https://doi.org/10.1016/j.cemconres.2024.107480.

#### References

- [1] Energy, B.S.R.o.W., 8th July, 2021.
- [2] J. Rogelj, et al., Scenarios towards limiting global mean temperature increase below 1.5 C, Nat. Clim. Chang. 8 (4) (2018) 325–332.
- [3] D.S. Siqueira, et al., Current perspectives on nuclear energy as a global climate change mitigation option, Mitig. Adapt. Strateg. Glob. Chang. 24 (5) (2019) 749–777.
- [4] I.A.E. Agency, Energy, Electricity and Nuclear Power Estimates for the Period up to 2050, Vienna, 2020.
- [5] K.H. Yano, et al., Investing in a permanent and sustainable nuclear waste disposal solution, Prog. Nucl. Energy 108 (2018) 474–479.
- [6] B.J. Riley, et al., Materials and processes for the effective capture and
- immobilization of radioiodine: a review, J. Nucl. Mater. 470 (2016) 307–326.
   J.S. McCloy, A. Goel, Glass-ceramics for nuclear-waste immobilization, MRS Bull. 42 (3) (2017) 233–240.
- [8] J. Huve, et al., Porous sorbents for the capture of radioactive iodine compounds: a review, RSC Adv. 8 (51) (2018) 29248–29273.
- [9] R.T. Jubin, Airborne Waste Management Technology Applicable for Use in Reprocessing Plants for Control of Iodine and Other off-Gas Constituents, Oak Ridge National Lab, TN (USA), 1988.
- [10] D.W. Holladay, Literature Survey: Methods for the Removal of Iodine Species from Off-gases and Liquid Waste Streams of Nuclear Power and Nuclear Fuel Reprocessing Plants, with Emphasis on Solid Sorbents, 1979.
- [11] Y. Watanabe, et al., Novel long-term immobilization method for radioactive iodine-129 using a zeolite/apatite composite sintered body, ACS Appl. Mater. Interfaces 1 (7) (2009) 1579–1584.
- [12] I. Publications, Treatment, Conditioning and Disposal of Iodine-129, International Atomic Energy Agency, Vienna, 1987.
- [13] E.D. Collins, et al., State-of-the-Art Report on the Progress of Nuclear Fuel Cycle Chemistry, Organisation for Economic Co-Operation and Development, 2018.
- [14] T.J. Robshaw, et al., Capture of aqueous radioiodine species by metallated adsorbents from wastestreams of the nuclear power industry: a review, SN Applied Sciences 3 (11) (2021) 1–15.
- [15] T.J. Robshaw, S. Kearney, J. Turner, M. Simoni, A. Baidak, C.A. Sharrad, B. Walkley, M.D. Ogden, Radioiodine abatement – Development of radioiodine targeting strategies in the light of zero emission, Prog. Nucl. Energy. ISSN: 0149-1970 165 (2023) 104918, https://doi.org/10.1016/j.pnucene.2023.104918.
- [16] Mukunoki, A., et al. Further development of iodine immobilization technique by low temperature vitrification with BiPbO2I.
- [17] J. Matyáš, et al., Silica-based waste form for immobilization of iodine from reprocessing plant off-gas streams, J. Nucl. Mater. 476 (2016) 255–261.
- [18] D.I. Kaplan, et al., Iodine speciation in a silver-amended cementitious system, Environ. Int. 126 (2019) 576–584.
- [19] M.I. Ojovan, W.E. Lee, S.N. Kalmykov, An Introduction to Nuclear Waste Immobilisation, Elsevier, 2019.
- [20] N.D.M. Evans, Binding mechanisms of radionuclides to cement, Cem. Concr. Res. 38 (4) (2008) 543–553.
- [21] L. Aimoz, et al., Characterization and solubility determination of the solid-solution between AFm-I 2 and AFm-SO 4, in: Cement-Based Materials for Nuclear Waste Storage, Springer, 2013, pp. 57–65.
- [22] M.L.D. Gougar, B.E. Scheetz, D.M. Roy, Ettringite and CoSoH Portland cement phases for waste ion immobilization: a review, Waste Manag. 16 (4) (1996) 295–303.
- [25] D.M. Strachan, H. Babad, Iodide and Iodate Sodalites for the Long-term Storage of Iodine-129, Rockwell International Corp., Richland, WA (USA), 1979. Rockwell Hanford Operations.
- [26] G.P. Sheppard, et al., Silver zeolites: iodide occlusion and conversion to sodalite-a potential 129I waste form? MRS Online Proc. Libr. 932 (1) (2006) 1–8.
- [27] T.J. Robshaw, et al., Functionality screening to help design effective materials for radioiodine abatement, Frontiers in Chemistry (2022) 10.
- [28] S. Kearney, et al., Encapsulation of iodine-loaded metallated silica materials by a geopolymer matrix, MRS Advances 7 (5) (2022) 105–109.
   [29] N.D. Authority, Geological Disposal RWM HAW Innovation and Delivery: A
- [29] N.D. Authority, Geological Disposal RWM HAW Innovation and Delivery: A Review of Cement Powders Security and Supply, Specifications and Disposability Issues, 2016, p. 144.

- [30] C.C. Castellano, et al., The effect of w/b and temperature on the hydration and strength of blastfurnace slag cements, Constr. Build. Mater. 111 (2016) 679–688.
- [31] S.A. Bernal, et al., Mechanical and thermal characterisation of geopolymers based on silicate-activated metakaolin/slag blends, J. Mater. Sci. 46 (16) (2011) 5477–5486
- [32] E. Özbay, M. Erdemir, H.İ. Durmuş, Utilization and efficiency of ground granulated blast furnace slag on concrete properties—a review, Constr. Build. Mater. 105 (2016) 423–434.
- [33] Roy, D.M. Hydration, structure, and properties of blast furnace slag cements, mortars, and concrete.
- [34] M. Buljac, et al., Voltammetric electrochemical behavior of carbon paste electrode containing intrinsic silver for determination of cysteine, Chemosensors 10 (7) (2022) 240.
- [35] A. Rigo, et al., Interaction of copper with cysteine: stability of cuprous complexes and catalytic role of cupric ions in anaerobic thiol oxidation, J. Inorg. Biochem. 98 (9) (2004) 1495–1501.
- [36] P. Duxson, et al., Geopolymer technology: the current state of the art, J. Mater. Sci. 42 (9) (2007) 2917–2933.
- [37] H.F.W. Taylor, Cement Chemistry 2nd Edition, 1997, 0727725920, 9780727725929.
- [38] L. Xu, et al., Recent advances in molecular dynamics simulation of the NASH geopolymer system: modeling, structural analysis, and dynamics, Constr. Build. Mater. (2021) 276.
- [39] J. Zhang, et al., Reinvestigation of dehydration and dehydroxylation of hydrotalcite-like compounds through combined TG-DTA-MS analyses, J. Phys. Chem. C 114 (24) (2010) 10768–10774.
- [40] J. Zelić, D. Rušić, R. Krstulović, Kinetic analysis of thermal decomposition of Ca (OH) 2 formed during hydration of commercial Portland cement by DSC, J. Therm. Anal. Calorim. 67 (3) (2002) 613–622.
- [41] S.A. Bernal, et al., Effect of silicate modulus and metakaolin incorporation on the carbonation of alkali silicate-activated slags, Cem. Concr. Res. 40 (6) (2010) 898–907.
- [42] L.R. Caballero, et al., Thermal, mechanical and microstructural analysis of metakaolin based geopolymers, Mater. Res. 22 (2019).
- [43] N.J. Saikia, et al., Cementitious properties of metakaolin-normal Portland cement mixture in the presence of petroleum effluent treatment plant sludge, Cem. Concr. Res. 32 (11) (2002) 1717–1724.
- [44] G. Engelhardt, D. Michel, High-resolution Solid-state NMR of Silicates and Zeolites, 1987.
- [45] D.E. Angulo-Ramírez, R.M. de Gutiérrez, F. Puertas, Alkali-activated Portland blast-furnace slag cement: mechanical properties and hydration, Constr. Build. Mater. 140 (2017) 119–128.
- [46] B. Walkley, et al., Activator anion influences the nanostructure of alkali-activated slag cements, J. Phys. Chem. C 125 (37) (2021) 20727–20739.
- [47] B. Walkley, J.L. Provis, Solid-state nuclear magnetic resonance spectroscopy of cements, Materials Today Advances 1 (2019) 100007.
- [48] P. Duxson, et al., 29Si NMR study of structural ordering in aluminosilicate geopolymer gels, Langmuir 21 (7) (2005) 3028–3036.
- [49] B. Walkley, et al., Incorporation of strontium and calcium in geopolymer gels, J. Hazard. Mater. 382 (2020) 121015.
- [50] Z. Dai, T.T. Tran, J. Skibsted, Aluminum Incorporation in the C–S–H phase of white Portland cement–metakaolin blends studied by 27 Al and 29 Si MAS NMR spectroscopy, J. Am. Ceram. Soc. 97 (8) (2014) 2662–2671.
- [51] J.F. Stebbins, et al., Quantification of five-and six-coordinated aluminum ions in aluminosilicate and fluoride-containing glasses by high-field, high-resolution 27Al NMR, J. Non-Cryst. Solids 275 (1–2) (2000) 1–6.
- [52] Nilforoushan, M.R., S. Otroj, and N. Talebian, The study of ion adsorption by amorphous blast furnace slag. 2015.
- [53] I.G. Lodeiro, et al., Effect on fresh CSH gels of the simultaneous addition of alkali and aluminium, Cem. Concr. Res. 40 (1) (2010) 27–32.
- [54] P. Yu, et al., Structure of calcium silicate hydrate (C-S-H): near-, mid-, and far-infrared spectroscopy, J. Am. Ceram. Soc. 82 (3) (1999) 742–748.
- [55] S. Boonjaeng, P. Chindaprasirt, K. Pimraksa, Lime-calcined clay materials with alkaline activation: phase development and reaction transition zone, Appl. Clay Sci. 95 (2014) 357–364.
- [56] C.E. White, et al., Combining density functional theory (DFT) and pair distribution function (PDF) analysis to solve the structure of metastable materials: the case of metakaolin, Phys. Chem. Chem. Phys. 12 (13) (2010) 3239–3245.
- [57] N.D. Authority, Geological Disposal: Near-field Evolution Status Report, 2010. NDA Report NDA/RWMD/033.
- [58] Society, A.N., Measurement of the leachibility of solidified low-level radioactive wastes by a short-term test procedure, ANSI/ANS 16 (2003) 1.
- [59] R.M. Asmussen, et al., Silver-based getters for 129I removal from low-activity waste, Radiochim. Acta 104 (12) (2016) 905–913.
- [60] J.G. Jang, S.M. Park, H.-K. Lee, Physical barrier effect of geopolymeric waste form on diffusivity of cesium and strontium, J. Hazard. Mater. 318 (2016) 339–346.
- [61] S.E. Pepper, et al., Iodine behaviour in spent nuclear fuel dissolution, Prog. Nucl. Energy 169 (2024) 105062.
- [62] B. Clément, et al., State of the Art Report on Iodine Chemistry, Organisation for Economic Co-Operation and Development, 2007.
- [63] G. Schmitz, Inorganic reactions of iodine(+1) in acidic solutions, Int. J. Chem. Kinet. 36 (9) (2004) 480–493.
- [64] Mohamed, R., R. Abd Razak, and M.M. Al Bakri Abdullah. A review on heat released in early geopolymerization by calorimetric study. Trans Tech Publ.